



INSTITUT DE FRANCE
Académie des sciences

Comptes Rendus


Chimie

Sonia Mancipe, Valentina Coca, Juan-Carlos Castillo, Hugo Rojas, María Helena Brijaldo, Claudia Castañeda, José Jobanny Martínez and Gustavo Pablo Romanelli

Synthesis of acrylonitrile functionalized hydroxymethylfurfural derivatives with $\text{Mg}(\text{OH})_2$ under solvent-free conditions

Volume 1, issue 0 (0000), p. 000-000

<https://doi.org/10.5802/crchim.239>

 This article is licensed under the
CREATIVE COMMONS ATTRIBUTION 4.0 INTERNATIONAL LICENSE.
<http://creativecommons.org/licenses/by/4.0/>



*Les Comptes Rendus. Chimie sont membres du
Centre Mersenne pour l'édition scientifique ouverte*

www.centre-mersenne.org

e-ISSN : 1878-1543



Research article

Synthesis of acrylonitrile functionalized hydroxymethylfurfural derivatives with $Mg(OH)_2$ under solvent-free conditions

Sonia Mancipe^{®*},^a, Valentina Coca^a, Juan-Carlos Castillo[®]^a, Hugo Rojas[®]^a,
María Helena Brijaldo[®]^b, Claudia Castañeda[®]^a, José Jobanny Martínez[®]^a
and Gustavo Pablo Romanelli[®]^{c, d}

^a Escuela de Ciencias Química-Grupo de Catálisis, Universidad Pedagógica y Tecnológica de Colombia, Avenida Central del Norte 39-115, Tunja, Colombia

^b Escuela de Ciencias Administrativas y Económicas- Grupo de Investigación de Farmacia y Medio Ambiente (FARQUIMA), Universidad Pedagógica y Tecnológica de Colombia, Avenida Central del Norte 39-115, Tunja, Colombia

^c Centro de Investigación y Desarrollo en Ciencias Aplicadas "Dr. Jorge J. Ronco" (CINDECA-CCT La Plata-CONICET-CIC-PBA), Universidad Nacional de La Plata, Calle 47 No 257, B1900AJK La Plata, Argentina

^d Centro de Investigación en Sanidad Vegetal (CISaV) / Cátedra de Química Orgánica, Facultad de Ciencias Agrarias y Forestales, Universidad Nacional de La Plata, Calles 60 y 119 s/n, B1904AAN La Plata, Argentina

E-mails: sonia.mancipe@uptc.edu.co (S. Mancipe), diana.coca01@uptc.edu.co (V. Coca), juan.castillo06@uptc.edu.co (J.-C. Castillo), hugo.rojas@uptc.edu.co (H. Rojas), maria.brijaldo@uptc.edu.co (M. H. Brijaldo), claudia.castaneda@uptc.edu.co (C. Castañeda), jose.martinez@uptc.edu.co (J. J. Martínez), gpr@quimica.unlp.edu.ar (G. P. Romanelli)

Abstract. Hydroxymethylfurfural (HMF) derivatives that contain an acrylonitrile group result in interesting scaffold molecules that can be obtained from biomass. However, the synthesis of these types of molecules has not been extensively studied. In this study, we investigated the catalytic activity of $Mg(OH)_2$ and MgO materials. Specifically, we evaluated the Knoevenagel reaction between HMF and malononitrile as a test reaction under solvent-free conditions. The fresh and used catalysts were evaluated using various techniques. Our results indicate that the combination of synthesis methods influences the crystalline, basic, and textural properties of the catalysts. We found that water plays an essential role in obtaining high yields. By using this simple and inexpensive method, we were able to achieve yields near 90% in short reaction times (<30 min).

Keywords. HMF, Active methylene, Brucite, Solvent-free, Knoevenagel reaction.

Funding. SM acknowledge the financial support from the Universidad Pedagógica y Tecnológica de Colombia (Internal Grant SGI-3344).

Manuscript received 5 April 2023, accepted 28 June 2023.

* Corresponding author.

1. Introduction

For several years, the primary source of carbon for obtaining fuels and chemical products was fossil fuels. However, at present, biomass has become one of the main sources of carbon, in particular carbohydrates such as glucose and fructose that present the largest natural basis of carbon [1]. The dehydration of fructose in an acid medium produces the preferential formation of 5-hydroxymethylfurfural (5-HMF). This substance is one of the most promoted platform chemicals derived from biomass, due to the variety of applications that are provided by the presence of hydroxyl, aldehyde, and furan moieties [2]. 5-HMF is widely used as an intermediate in pharmaceutical products, flavor enhancers in the food industry and for the synthesis of polymers [3]. Many efforts have focused on the organic synthesis of HMF derivatives with active methylene compounds in order to obtain high-value-added products through environmentally friendly catalysts and renewable raw materials [4]. However, these classical reactions have been scarcely studied using 5-HMF. Among them, the Knoevenagel condensation is one of the important reactions for obtaining C–C bonds [5]. This reaction is a typical base-catalyzed reaction that involves the abstraction of a proton from activated methylene by basic sites to obtain the corresponding carbanion. Studying basic solid materials in these reactions has made it possible to contribute to green and sustainable chemistry [6]. Hydrotalcite (HT) or hydrotalcite-like compounds are commonly employed as base catalysts [7]. However, Knoevenagel condensation reactions over metal oxide catalysts have been less investigated [8], although these materials can be easily obtained at lower costs than hydrotalcite-type compounds.

MgO and $\text{Mg}(\text{OH})_2$ are well known to be basic and inexpensive solids that have been used as catalysts for a wide variety of organic transformations including oxidation, reduction, epoxidation, condensation, and notable heterocyclic reactions [9,10]. MgO exhibits good catalytic activity in the Knoevenagel condensation depending on the method and conditions of its preparation which affects their surface and which can lead to increased CO_2 chemisorption and higher concentration of strong basic sites [11,12]. To increase the catalytic activity of MgO, which has a low surface area (near $20 \text{ m}^2/\text{g}$) and low concentration

of basic sites (around 0.4 mmol/g), it is supported on materials such as carbon [13], Al-MCM-41 [14], ZrO_2 [15], or also by modifying the synthesis of MgO using surfactants (sol–gel method), with the thermal treatment of $\text{Mg}(\text{OH})_2$, or using hydration–dehydration procedures which alter surface characteristics of MgO [12].

In the sol–gel synthesis, it has been observed that the crystallinity of the magnesium oxide depends on the surfactant concentration used [11], and consequently, the Knoevenagel condensation of benzaldehyde with ethyl cyanoacetate using MgO prepared with the highest surfactant concentration (Pluronic P123) led to the highest catalytic activity due to the highest quantity of basic sites.

The simple calcination of precursors as rehydrated $\text{Mg}(\text{OH})_2$ allows obtaining MgO with a high surface area and activity for base-catalyzed reactions [16]. Temperatures between 350 and $450 \text{ }^\circ\text{C}$ are sufficient to obtain surface areas of about $300 \text{ m}^2/\text{g}$. The formation of a particle-internal nanostructure comprised of newly crystallized strictly aligned, cube-shaped, and nanometer-sized crystals of MgO is the main cause of this increase in the surface area [17].

The basic sites can be controlled by the densified nanostructured MgO material in the synthesis method [18] due to the creation of atomic disorder formed at the interface of crystal grains (grain boundaries) between MgO nanocrystals. Another strategy used was the use of MgO-stabilized Pickering emulsion. Sadgar *et al.* [19] studied the emulsion-stabilizing ability of MgO depending on the method of preparation, calcination temperature, and solvents. These authors found that the high emulsion stability and small droplet size have a considerable effect on the catalytic activity in the Knoevenagel condensation. For the adduct condensation of furfural and methylene compounds such as malononitrile, it has been reported that it almost always requires short times of reaction using MgO or $\text{Mg}(\text{OH})_2$ (15 min, yield > 83) [20] and lower temperatures of reaction ($20 \text{ }^\circ\text{C}$ in 5 min) to reach yields of 96% [21]. However, no report has been described for obtaining hydroxymethylfurfural (HMF) derivatives containing an acrylonitrile moiety which could result in interesting molecules obtained from biomass.

Curiously, the Knoevenagel condensation between HMF and malononitrile has only been

described by three research groups. Rani *et al.* [22] described the use of an amine-functionalized MOF (UiO-66-NH₂) to obtain quantitative yields of the adduct HMF with malononitrile. Mancipe *et al.* [23], used hydrotalcite doped with boric acid allowing to obtain yields near 86%, while imidazole-functionalized 3D-cobalt metal-organic framework led to quantitative yields under mild reaction conditions (40 °C in 30 min). The absence of a catalyst requires that the Knoevenagel reactions occur at higher temperatures for prolonged times of reaction to afford the adduct in only 30% yield [24].

The Mg²⁺ cation and O²⁻ anion can be considered as an acid-base pair [12] leading to the preferential formation of Knoevenagel products. However, some studies highlighted the importance of the hydroxyls on the MgO surface to stabilize the generated anionic intermediate R⁻ after abstraction of the proton [25]. For this reason, the presence of MgO and Mg(OH)₂ materials for the solventless Knoevenagel condensation of HMF and malononitrile was studied.

2. Experimental section

2.1. Preparation of Mg(OH)₂ and MgO

For the synthesis of magnesium hydroxide by the precipitation method, the magnesium precursor solution (0.0857 mol of Mg(NO₃)₂·6H₂O) was placed in a glass reactor containing an alkaline solution (0.1715 mol of NaOH); the solutions were simultaneously left under permanent agitation and aged for one day at room temperature. The suspension was washed several times with distilled water and dried at 80 °C. The obtained solid was named BPC.

Mg(OH)₂ by sol-gel method was synthesized using 10 mL of CTAB (cetyltrimethylammonium bromide) as a cationic surfactant. This was added with constant stirring to a 1 M solution of Mg(NO₃)₂·6H₂O for one hour. After this time, a 1 M ammonia solution was added dropwise until the clear solution forms the Mg(OH)₂ sol. The sol was left to age for 2 days so that the sol particles condense in the gel. The gel particles were collected by filtering and washing the material several times with distilled water, and the final product denominated BSG was dried at 80 °C.

In both cases, for obtaining the magnesium oxides, the hydroxides synthesized by precipitation and

sol-gel methods were calcined at 500 °C and named MPC and MSG, respectively.

2.2. Characterizations

X-ray powder diffraction patterns (XRD) of the catalysts were recorded with a PANalytical diffractometer model X'PERT-PRO with Co K α radiation (λ = 1.78901 Å) and a 1D pixel detector. The data were collected with a step increment of 0.013° in the range of 5° ≤ Θ ≤ 80°.

FTIR spectra were obtained by the ATR method using a Thermo SCIENTIFIC model NICOLET iS50 FT-IR equipment with a wavenumber range of 4000–400 cm⁻¹ and a resolution of 4 cm⁻¹.

XPS analysis was obtained using a Thermo Scientific ESCALAB 250 XI photoelectron spectrometer with a step of 0.05 eV, pass energy of 25 eV, and dwell time of 50 ms. The pressure was kept around 10⁻⁸ mbar inside the analysis chamber. The spectra were calibrated employing the C 1s peak (284.4 eV).

For the textural analysis measurements, a Micromeritics ASAP 2020 equipment was used. The samples were previously degassed at 250 °C for 4 h with a vacuum of 10⁻³ mmHg to eliminate gases or molecules adsorbed on the surface. Nitrogen adsorption-desorption isotherms were measured at -193.15 °C, obtaining data on the volume of adsorbed gas (cm³ STP/g sample) versus the relative pressure of nitrogen (P/P_0).

CO₂ adsorption was measured by the DRIFTS method using a Thermo SCIENTIFIC model NICOLET iS50 FT-IR spectrometer. The oxides and hydroxides were prepared with a 30 mL/min flow of He at 100 °C for 30 min. After the flow of He, the adsorption of CO₂ was evaluated at room temperature. DRIFT spectra of the CO₂-adsorbed species on the surface were obtained by subtracting the background spectra.

NMR spectra were recorded on a Bruker Avance 400 spectrophotometer (Bruker BioSpin GmbH, Rheinstetten, Germany), operating at 400.1 MHz (¹H) and 100.6 MHz (¹³C) at 298 K using tetramethylsilane (0 ppm) as the internal reference. NMR spectroscopic data were recorded in CDCl₃ using as internal standards the residual non-deuterated signal (δ = 7.26 ppm) for ¹H NMR and the deuterated solvent signal (δ = 77.16 ppm) for ¹³C{¹H} NMR spectroscopy. Chemical shifts (δ) and coupling constants (J) are given in ppm and Hz, respectively.

2.3. Catalytic studies

Mg(OH)₂ and MgO synthesized by precipitation and sol-gel methods were studied in the solventless synthesis of the Knoevenagel reaction. A mixture of 5-(hydroxymethyl)furfural (0.4 mmol), malononitrile (0.4 mmol), and catalyst (20 mg) was placed in a glass tube with constant stirring. Under solvent-free conditions, the tube was heated to 60 °C for 3 h. Once the reaction was finished, 2.0 mL of ethyl acetate was added to solubilize the Knoevenagel product and the catalyst was readily recovered by simple filtration. The monitoring of the reaction was done in a gas chromatograph coupled to mass spectroscopy (GC-MS), using a column HP-5. A sample was purified by a flash chromatography column on silica gel using dichloromethane as an eluent to afford 2-((5-(hydroxymethyl)furan-2-yl)methylene)malononitrile **3a**. Brown solid. R_f = 0.16 (DCM). M.p. 76–77 °C (amorphous). ¹H NMR (400 MHz, CDCl₃): δ = 2.85 (br s, 1H, OH), 4.73 (s, 2H), 6.62 (d, *J* = 3.6 Hz, 1H), 7.27 (d, *J* = 3.6 Hz, 1H), 7.46 (s, 1H) ppm. ¹³C{¹H} NMR (101 MHz, CDCl₃): δ = 57.6 (CH₂), 112.0 (CH), 113.0 (C), 114.0 (C), 125.2 (CH), 142.9 (CH), 147.7 (C), 162.6 (C) ppm.

3. Results and discussion

3.1. Characterization

The structural phase of MgO and Mg(OH)₂ was determined by XRD. Figure 1 shows the diffraction patterns for MgO at 36.6°, 42.90°, 62.30°, 74.9°, and 78.5° in 2θ for (111), (200), (220), (311), and (222) planes, respectively [26]. The crystalline phase of MgO corresponds to cubic structure (lattice parameters *a*, *b*, *c* = 4.2130 Å) with space group Fm3m (JCPDS card 45-0946) [27]. The sharp peaks indicate the presence of well-crystallized MgO particles under precipitation and sol-gel synthesis conditions. X-ray diffraction patterns for magnesium hydroxide are dependent on crystalline Mg(OH)₂ nanoparticles [28], and the planes can be indexed as a hexagonal structure with space group P-3m1 and lattice parameters *a* of 3.1442 Å and *c* of 4.7770 Å (JCPDS card 07-0239) [29,30]. In the MPC material, a signal is shown at 30° in 2θ, which can be attributed to a change from brucite to a pseudomorphic periclase that originates once the dehydroxylation ends [31]. The average crystallite size of the catalysts evaluated from

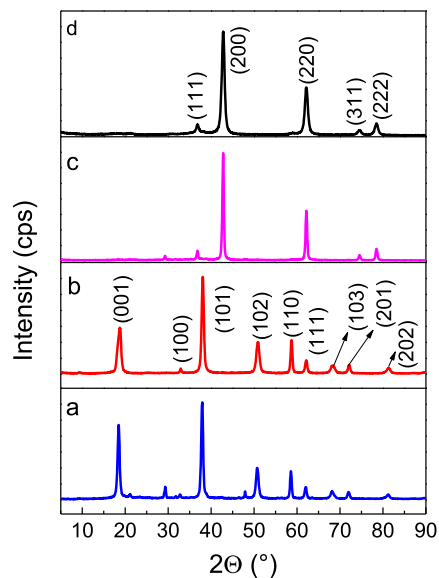


Figure 1. X-ray diffraction of (a) BSG, (b) BPC, (c) MSG, (d) MPC.

diffraction planes was measured using the Scherrer equation. The values of BPC, BSG, MPC, and MSG are 12.56, 15.27, 9.71, and 19.54 nm, respectively, showing slightly larger crystallite size in solids synthesized by sol-gel than those prepared by the precipitation method.

The FTIR spectra of Mg(OH)₂ and MgO materials synthesized by sol-gel and precipitation methods are shown in Figure 2. The hydroxides present an intense peak at 3700 cm⁻¹ due to the OH stretching vibrations in Mg(OH)₂ [32]. It is known that MgO can chemisorb H₂O and CO₂ on the surface; the signal around 1400 cm⁻¹ may correspond to carbonate ions (CO₃²⁻) adsorbed on the surface, even after the calcination process [33]. In the Mg(OH)₂ sol-gel catalyst, the signals at 2918 and 2858 cm⁻¹ correspond to asymmetric ν_{as}(CH₃) [34]. The band at 3700 cm⁻¹ disappears in the spectrum of the calcined sample, which is due to the decomposition of Mg(OH)₂ to MgO particles. The bands below 1000 cm⁻¹ correspond to M–O and M–OH (M = metal) characteristics of Mg–O and Mg–OH, respectively.

Table 1 summarizes the binding energies and ratios of signals of Mg 1s and O 1s. The XPS spectra are shown in Figure 3. The signal characteristics of Mg(OH)₂, MgO, and Mg(NO₃)₂ are observed at 1303.08 eV and 1304.48 eV, and 1305 eV, respectively [35]. The proportion of these signals depends

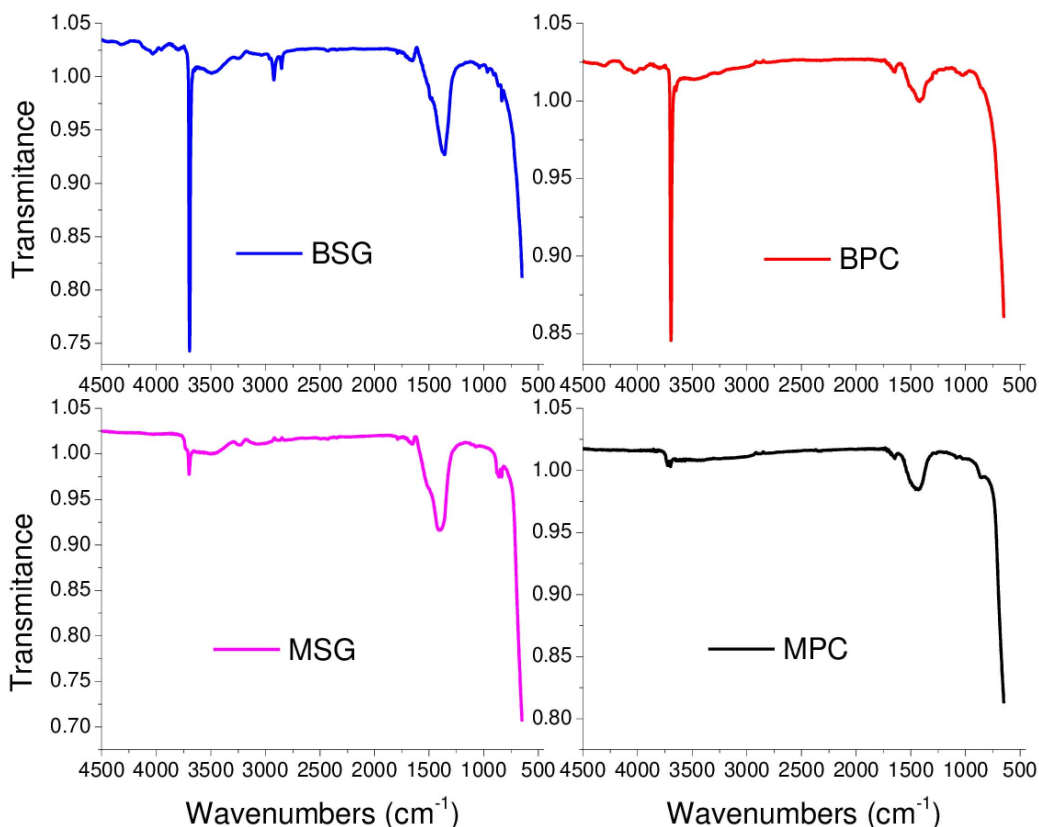


Figure 2. FTIR spectra of synthesized materials.

on the method of preparation and consequently on the calcination temperature. Thus, $\text{Mg}(\text{OH})_2$ was only observed in sol-gel synthesis. This is consistent with X-ray diffraction results. The precipitation method allows obtaining a mixture of $\text{Mg}(\text{OH})_2$, and the precursor used $\text{Mg}(\text{NO}_3)_2$. Once the calcination takes place at 500 °C, the proportion of MgO and Mg^{2+} is dependent on the method employed. A shift to the highest binding energy could indicate the highest proportion of Mg^{2+} species on the surface. The binding energies of the signals assigned to oxygen in lattices (O_b) and oxygen in OH groups (O_s) are shown in Table 1. The quantitative ratio O_b/O_s shows that the precipitation method favors the formation of bulk oxygen in $\text{Mg}(\text{OH})_2$, which could be related to the lowest hydration of brucite obtained for this method. This ratio drops when MgO is formed by calcination from $\text{Mg}(\text{OH})_2$, but this same behavior is observed in the ratio between the two main signals. In

consequence, it is possible to suppose that the sol-gel method favors the hydration of brucite and MgO on the surface.

In the textural analysis, the specific surface area (S_{BET}) of the solids $\text{Mg}(\text{OH})_2$ and MgO is shown in Table 1. No evident changes are observed before and after the calcination process in the S_{BET} values. The nitrogen adsorption-desorption isotherms are characteristics of type IV with H4 hysteresis loop [32], showing sharp peaks at high relative pressures, indicating that the materials contain large mesopores and macropores, which can be verified in the pore size distribution. In general, the precipitation method to obtain $\text{Mg}(\text{OH})_2$ led to the highest density of pores (dV/dD) with a minor pore diameter compared with sol-gel synthesis (Figure 4). Besides, the calcination of $\text{Mg}(\text{OH})_2$ sol-gel showed a broad pore diameter. This means that the porosity is highly dependent on the synthesis method and calcination process.

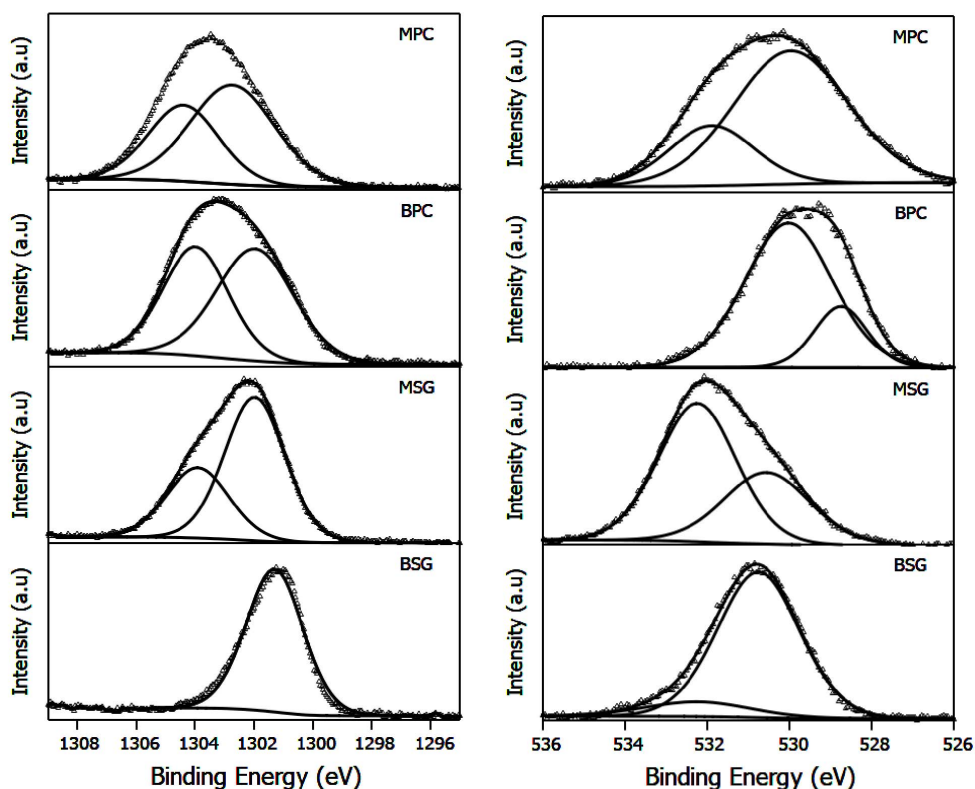


Figure 3. XPS spectra of Mg 1s and O 1s for Mg(OH)₂ and MgO materials.

Table 1. Binding energies of Mg 1s and O 1s, quantitative ratio O_b/O_s and O 1s/Mg 1s, and surface area (S_{BET}) and pore size

Catalyst	Mg 1s	O 1s	O_b/O_s^*	O 1s/Mg 1s	S_{BET} (m ² /g)	Pore size (nm)
BSG	1301.7(66),	532.2(64),	1.77	0.08	25	22.4
	1300.8(34)	530.56(36)				
BPC	1303.9(44),	530.05(79),	3.76	0.42	35	33.7
	1301.6(56)	528.75(21)				
MSG	1302.9(63),	532.2(12),	0.13	0.16	26	14.8
	1304.8(37)	530.7(88)				
MPC	1304.47(29),	531.85(25),	0.33	0.24	35	22.3
	1302.89(71)	529.97(75)				

* O_b/O_s quantitative ratio between bulk and surface oxygen.

CO₂ adsorption followed by DRIFT spectra of MgO and Mg(OH)₂ synthesized by the two methods is shown in Figure 5. In the spectra taken at room temperature, signals can be observed between 3800 and 3300 cm⁻¹ corresponding to the hydroxyl groups

on the surface that may be in variable coordination with the cation, while the signal at 800 cm⁻¹ may be due to the bulk infrared absorption of MgO [36]. With the adsorption of CO₂, the formation of monodentate species can be seen at 1572, 1501, and 1411 cm⁻¹.

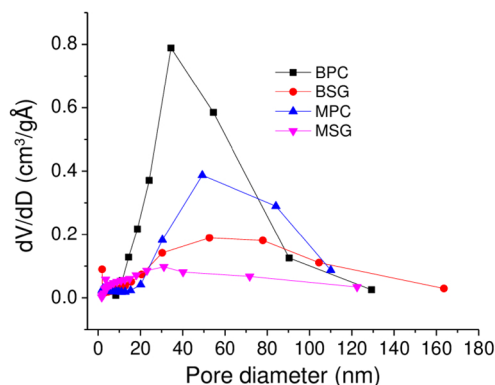


Figure 4. BJH pore size distribution curves of Mg(OH)₂ and MgO materials.

The signals at 1647 and 1331 cm⁻¹ can be assigned to bidentate species [37]. In the adsorption process, CO₂ chemisorbs on the active sites as unidentate, bidentate, and bridged carbonates; however, the formation of bidentate species is favored on the most active sites, reducing the number of free carbonate ions. The higher formation of bidentate species in Mg(OH)₂ can be explained by the fact that some of the active sites have conformational characteristics. Furthermore, this description is consistent with the fact that the bidentate carbonate is less basic than the unidentate and bridged carbonates [38]. Taking into account the aforementioned and according to Figure 5, it could be affirmed that MgO solids present a higher basicity in comparison with the hydroxides that show signs of adsorption of bidentate species. On the other hand, the signals at 2924 and 2854 cm⁻¹ in the magnesium hydroxide can be attributed to the H⁺ ions resulting from the dissociation of water molecules that can be trapped by the surface O²⁻ ions [39].

3.2. Evaluation of the catalytic activity

The Knoevenagel reaction between 5-HMF (1a) and malononitrile (2a) was studied as a test reaction under solvent-free conditions at 60 °C. The Knoevenagel adduct (3a, *m/z* = 174) formed by a condensation process and the aldehyde (3b, *m/z* = 172) obtained by the dehydrogenation of the hydroxyl group into adduct 3a were the main products observed (Scheme 1). Figures 6a and 6b display the yields of 3a and 3b, respectively, as the reaction

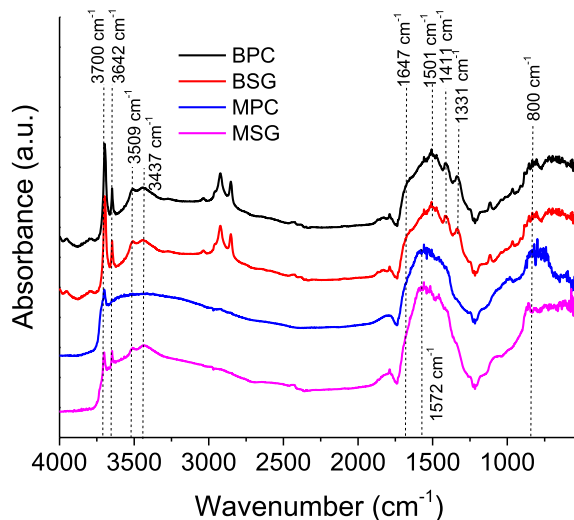
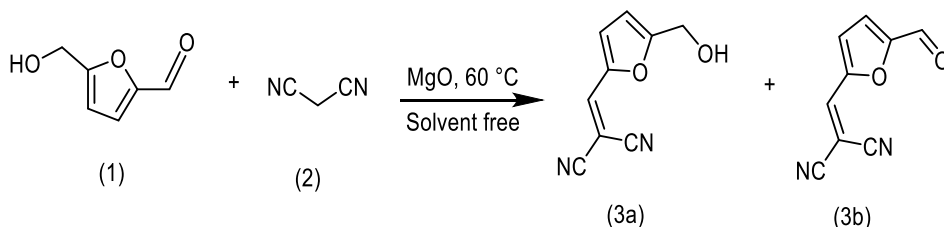


Figure 5. DRIFT spectra of MgO and Mg(OH)₂ materials at room temperature.

progresses with each catalyst used. It is observed that they show the preferential formation of adduct 3a with good yields. Although this reaction can typically be conducted in H₂O, in the absence of catalyst, and moderate temperatures, the Knoevenagel adduct is obtained in lower yields. Thus, the use of catalysts under solvent-free conditions appears interesting to understand the role of water on the surface of MgO.

It can be observed for the uncalcined and calcined catalysts that the catalytic behavior is highly dependent on the preparation method. The preferential formation of 3a is observed with Mg(OH)₂ obtained by the sol-gel synthesis. The Knoevenagel product 3a requires deprotonation of the α -methylene hydrogen atoms by basic sites. The hydroxyl groups on the surface of the solid stabilize the anionic intermediate formed on the surface [25]. BSG and BPC display a similar basicity but a distinct proportion of surface hydroxyls. Thus the catalysts with the lowest ratio of O_b/O_s present the highest yield for adduct 3a. However, the formation of the adduct 3b in moderate yields is unexpected. The lowest amount of surface hydroxyls and the presence of two phases of Mg²⁺ in BPC could favor the formation of adduct 3b, which can be formed by two pathways, including the faster formation of diformylfuran (DFF) that condenses with malononitrile or the dehydrogenation of adduct 3a.



Scheme 1. Products formed in the condensation of Knoevenagel between 5-HMF and malononitrile.

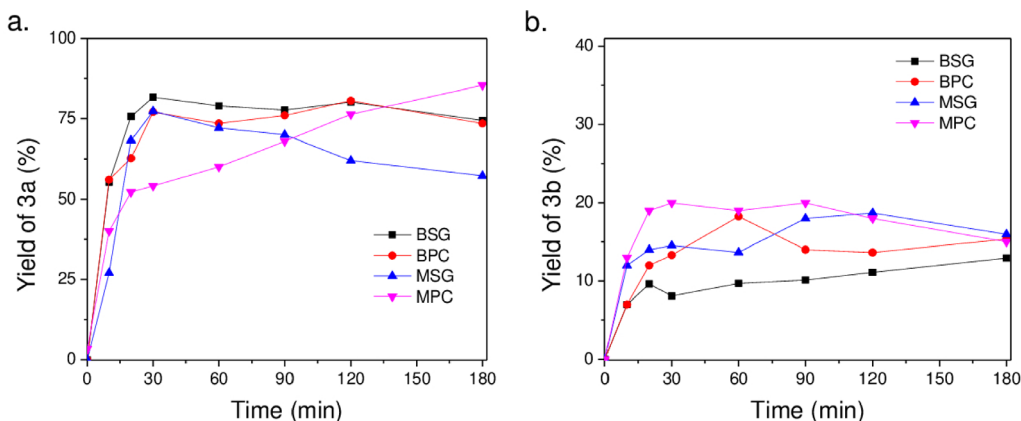


Figure 6. (a) Yield of 3a and (b) yield of 3b as a function of reaction time with MgO and Mg(OH)₂ materials at room temperature at 60 °C, 100 mg of catalyst, and 600 rpm.

MgO catalysts show a distinct behavior. As the reaction progresses and by release of water in the reaction medium, the catalyst surface is modified and the Knoevenagel reaction is consequently favored for MPC solid. This phenomenon was not observed with MSG, where the yield of adduct 3a drops, favoring the formation by dehydrogenation toward product 3b. These catalysts present the highest basicity and consequently could also favor the formation of this product. Thus, the role of surface hydroxyls in the reaction mechanism to obtain 3a is evident. The MSG catalyst with a higher proportion of surface hydroxyls shows a better performance toward the Knoevenagel reaction at the start of the reaction.

The effect of temperature was studied using MPC. An increase in temperature should avoid the presence of water on the surface favoring the formation of 3a, as can be observed in Figure 7. However, at the lowest temperatures, the reaction also allows the formation of 3b. In summary, the selectivity of the reaction could be controlled by surface hydroxyls due to the stabilization of anionic intermediates.

To confirm that those results were obtained without external mass transfer, the reaction was performed at different catalyst amounts (5–20 mg) at 60 °C for 24 h. As shown in Table 2 (entries 1–4), the behavior follows a linear trend when the catalyst mass is increased, suggesting the absence of external mass-transfer resistance. Besides, the recyclability of the MPC catalysts (entries 5–8) was studied by separation from the mixture by simple filtration, washing with hot acetone, and drying at 80 °C for 4 h. The catalyst was reused up to 4 times without appreciable loss of catalytic activity. In the fourth reuse, the mass loss of the catalyst was approximately 5%.

The structure of Knoevenagel adduct 3a was confirmed by ¹H and ¹³C{¹H} NMR spectroscopy (Figure 8). The ¹H NMR spectrum shows two singlets at 4.73 and 7.46 ppm assigned to methylenoxy (CH₂O) and vinyl (=CH) protons, respectively. To our delight, the proton signal of the hydroxyl group was observed at 2.85 ppm, indicating that the dehydrogenation of the CH₂OH moiety was not successful. The ¹³C{¹H} NMR spectrum of 3a displays eight

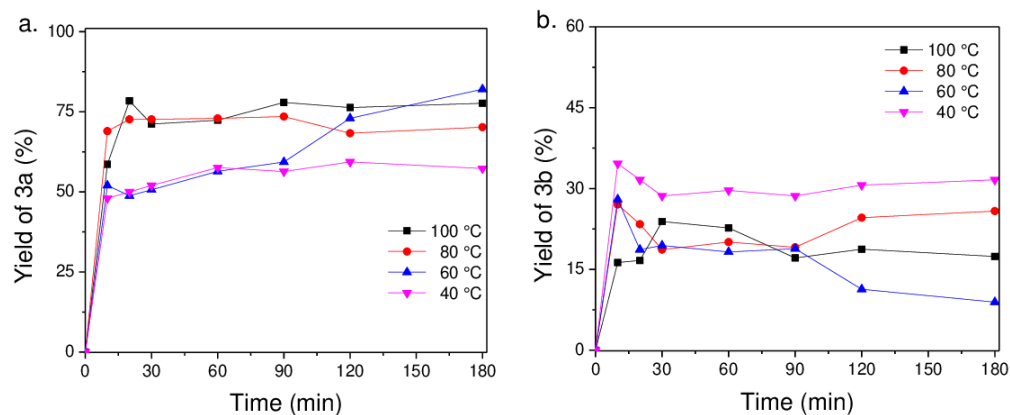


Figure 7. Effect of temperature in the Knoevenagel reaction with MPC (a) 3a adduct and (b) 3b product.

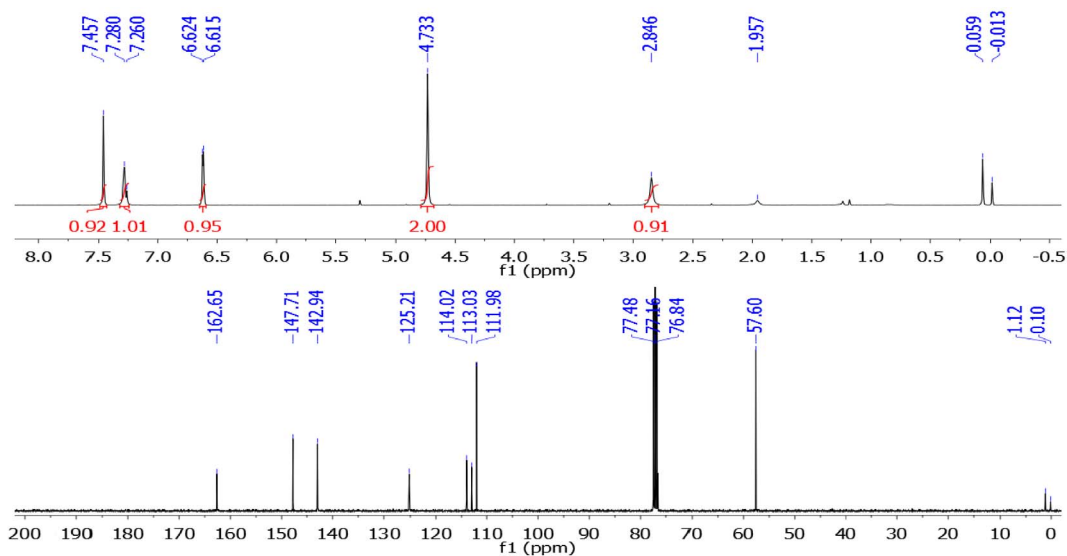


Figure 8. ^1H and $^{13}\text{C}\{^1\text{H}\}$ NMR spectra of the Knoevenagel adduct 3a.

Table 2. The recycling capability of MPC catalyst in the Knoevenagel synthesis of 3a at different catalyst amounts at 60 °C for 24 h

Entry	Catalysts	Loading (mg)	T (°C)	Time (h)	Reuse cycle	Yield (3a) (%)
1	MPC	5	60	24	–	50
2	MPC	10	60	24	–	60
3	MPC	15	60	24	–	68
4	MPC	20	60	24	–	77
5	MPC	20	60	24	1	77
6	MPC	20	60	24	2	75
7	MPC	20	60	24	3	70
8	MPC	20	60	24	4	68

carbon signals, consisting of one methylene, three methines, and four quaternary carbons. In particular, the methylenoxy (CH₂O) and vinylic (=CH) carbons can be observed at 57.6 and 142.9 ppm, respectively.

4. Conclusions

In the present study, the efficient synthesis of MgO and Mg(OH)₂ materials was carried out by the sol-gel and precipitation methods. The XRD characterization of the solids revealed formation of brucite and periclase phases. IR studies showed signals typical of hydroxyl groups and M–OH and M–O vibrations. The O_b/O_s ratios obtained from XPS analysis indicate that synthesis by precipitation results in a lower hydration of the brucite phase compared to the sol-gel method. The greater formation of bidentate species on the surface of Mg(OH)₂ indicates lower basicity compared to MgO. Finally, orienting the catalytic activity in the Knoevenagel condensation reaction between HMF and malononitrile under environmentally friendly solvent-free conditions toward the formation of product 3a requires the deprotonation of the α-methylene hydrogen atoms and catalysts with a lower O_b/O_s ratio present higher yield of adduct 3a. On the other hand, the lower presence of hydroxyls on the surface of BPC favors product 3b.

Conflicts of interest

Authors have no conflict of interest to declare.

References

- [1] W. Fan, Y. Queneau, F. Popowycz, *Green Chem.*, 2018, **20**, 485-492.
- [2] C. Afonso, R. Gomes, Y. Mitrev, S. Simeonov, *ChemSusChem*, 2018, **11**, 1612-1616.
- [3] X. Yue, Y. Queneau, *ChemSusChem*, 2022, **15**, article no. e202102660.
- [4] J. van Schijndel, L. A. Canalle, D. Molendijk, J. Meuldijk, *Synlett*, 2018, **29**, 1983-1988.
- [5] X. Li, B. Lin, H. Li, Q. Yu, Y. Ge, X. Jin, X. Liu, Y. Zhou, J. Xiao, *Appl. Catal. B*, 2018, **239**, 254-259.
- [6] A. Jadhav, G. Yadav, *J. Chem. Sci.*, 2019, **131**, 131-179.
- [7] W. Bing, H. Wang, L. Zheng, D. Rao, Y. Yang, L. Zheng, B. Wang, Y. Wang, M. Wei, *Green Chem.*, 2018, **20**, 3071-3080.
- [8] J. N. Appaturi, R. Ratti, B. L. Phoon, S. M. Batagarawa, I. U. Din, M. Selvaraj, R. J. Ramalingam, *Dalton Trans.*, 2021, **50**, 4445-4469.
- [9] A. Corma, S. Iborra, in *Optimization of Alkaline Earth Metal Oxide and Hydroxide Catalysts for Base-Catalyzed Reactions* (B. C. Gates, H. Knözinger, eds.), vol. 49, Academic Press, 2006, 239-302.
- [10] H. Dabhane, S. Ghotekar, P. Tambade, S. Pansambal, R. Oza, V. Medhane, *Eur. J. Chem.*, 2021, **12**, 86-108.
- [11] L. G. Possato, E. Pereira, R. G. L. Gonçalves, S. H. Pulcinelli, L. Martins, C. V. Santilli, *Catal. Today*, 2020, **344**, 52-58.
- [12] M. León, L. Faba, E. Díaz, S. Bennici, A. Vega, S. Ordóñez, A. Auroux, *Appl. Catal. B*, 2014, **147**, 796-804.
- [13] M. Godino-Ojer, A. J. López-Peinado, R. M. Martín-Aranda, J. Przepiórski, E. Pérez-Mayoral, E. Soriano, *ChemCatChem*, 2014, **6**, 3440-3447.
- [14] S. Karnjanakom, T. Suriya-umporn, A. Bayu, S. Kongparakul, C. Samart, C. Fushimi, A. Abudula, G. Guan, *Energy Convers. Manag.*, 2017, **142**, 272-285.
- [15] W. Shen, G. A. Tompsett, K. D. Hammond, R. Xing, F. Dogan, C. P. Grey, W. C. Conner, S. M. Auerbach, G. W. Huber, *Appl. Catal. A: Gen.*, 2011, **392**, 57-68.
- [16] C. Xu, J. Bartley, D. Enache, D. Knight, G. Hutchings, *Synthesis-Stuttgart*, 2005, **19**, 3468-3476.
- [17] H. Pimminger, G. Habler, N. Freiburger, R. Abart, *Phys. Chem. Miner.*, 2016, **43**, 59-68.
- [18] R. Vidruk, M. V. Landau, M. Herskowitz, M. Talianker, N. Frage, V. Ezersky, N. Froumin, *J. Catal.*, 2009, **263**, 196-204.
- [19] A. L. Sadgar, T. S. Deore, R. V. Jayaram, *ACS Omega*, 2020, **5**, 12224-12235.
- [20] M. Shirotori, S. Nishimura, K. Ebitani, *Catal. Sci. Technol.*, 2014, **4**, 971-978.
- [21] H. Moison, F. Texier-Boullet, A. Foucaud, *Tetrahedron*, 1987, **43**, 537-542.
- [22] P. Rani, R. Srivastava, *J. Colloid Interface Sci.*, 2019, **557**, 144-155.
- [23] S. Mancipe, J.-C. Castillo, M. H. Brijaldo, V. P. López, H. Rojas, M. A. Macías, J. Portilla, G. P. Romanelli, J. J. Martínez, R. Luque, *ACS Sustain. Chem. Eng.*, 2022, **10**, 12602-12612.
- [24] M. C. A. Carreira, M. C. Oliveira, A. C. Fernandes, *Mol. Catal.*, 2022, **518**, article no. 112094.
- [25] C. Chizallet, G. Costentin, H. Lauron-Pernot, J.-M. Krafft, P. Bazin, J. Saussey, F. Delbecq, P. Sautet, M. Che, *Oil Gas Sci. Technol. - Revue de l'IFP*, 2006, **61**, 479-488.
- [26] N. Clament Sagaya Selvam, R. Thinesh Kumar, L. John Kennedy, J. Judith Vijaya, *J. Alloys Compd.*, 2011, **509**, 9809-9815.
- [27] M. A. Alavi, A. Morsali, *Ultrason. Sonochem.*, 2010, **17**, 441-446.
- [28] K. Saoud, S. Saeed, R. Al-Soubaih, M. Bertino, *Am. J. Nanomater.*, 2014, **2**, 21-25.
- [29] S. Zavareh, F. Majedi, S. M. A. Sharif Sheikholeslami, F. Golestanifard, M. Esmailian, *Int. J. Nanosci.*, 2009, **8**, 565-569.
- [30] A. Ranaivosoloarimanana, T. Quiniou, M. Meyer, J. M. Boyer, F. Rocca, *Physica B: Condens. Matter*, 2009, **404**, 3655-3661.
- [31] R. Salomão, C. C. Arruda, M. L. P. Antunes, *InterCeram - Int. Ceram. Rev.*, 2020, **69**, 52-62.

- [32] Md. H. Zahir, M. M. Rahman, K. Irshad, M. M. Rahman, *Nano-materials*, 2019, **9**, article no. 1173.
- [33] A. Ansari, A. Ali, M. Asif, *New J. Chem.*, 2018, **42**, 184-197.
- [34] R. Kurrey, M. K. Deb, K. Shrivastava, *New J. Chem.*, 2019, **43**, 8109-8121.
- [35] C. D. Wagner, D. A. Zatko, R. H. Raymond, *Anal. Chem.*, 1980, **52**, 1445-1451.
- [36] C. A. Cadigan, A. R. Corpuz, F. Lin, C. M. Caskey, K. B. H. Finch, X. Wang, R. M. Richards, *Catal. Sci. Technol.*, 2013, **3**, 900-911.
- [37] D. Cornu, H. Guesmi, J.-M. Krafft, H. Lauron-Pernot, *J. Phys. Chem. C*, 2012, **116**, 6645-6654.
- [38] H. Du, C. T. Williams, A. D. Ebner, J. A. Ritter, *Chem. Mater.*, 2010, **22**, 3519-3526.
- [39] A. Kumar, J. Kumar, *Solid State Commun.*, 2008, **147**, 405-408.